A NEW 3D PARADIGM FOR METAL ARTIFACT REDUCTION IN DENTAL CT

V. Naranjo, R. Lloréns, M.Alcañiz[*] *R. Verdú-Monedero, J. Larrey-Ruiz, J. Morales-Sánchez*[†]

I3BH, Universidad Politécnica de Valencia
Valencia, Spain

Universidad Politécnica de Cartagena,
Cartagena, Spain

ABSTRACT

The presence of metal artifacts in dental CT prevents the correct exploration and planning of dental interventions. This paper addresses a new paradigm in metal artifact reduction that uses the backprojected data available in the DICOM files. The method, based on variational image registration and morphological lambda reconstruction, enhances the image quality using not only the information of the artifacted image (horizontal approach) but also the information of adjoining images (vertical approach). Some preliminary results involving different CT scanners and patients are presented and discussed.

Index Terms— Metal artifact reduction, dental CT, variational image registration, morphological lambda reconstruction

1. INTRODUCTION

CT scan has become a standard tool for medical examination. The data acquired from CT studies are usually reformatted in 2D images by means of the filtered back projection (FBP) method. When objects with high density are present in a CT scan, the method induces nonlinearities that have a highly negative impact on the images, giving rise to the appearance of radial patterns known as streaking and beam hardening. This is a common problem in dental CT due to the presence of dental fillings (usually gold or amalgam) and implants (usually titanium). At the same time, the use of computer applications for the diagnosis and the planning of dental surgery is usual among dentists and surgeons. These applications represent a 3D reconstruction of the patient's anatomy and allow the *ex vivo* exploration and manipulation of the data as well as the planning of the surgery. The metal artifacts make the visualization of the 2D sections difficult and distort the 3D reconstruction. A metal artifact reduction (MAR) processing is therefore needed to adapt the CT data to dental planning tools.

Most of the previous work in the MAR field use the CT raw data. There are several approaches to the problem. On one hand, some of them reconstruct the image with the FBP and detect the artifacted areas so as to replace that information. Kallender et al. [1] proposed a method to linearly interpolate the problematic data in the projection domain and then replace the affected image data. Afterwards, Watzke et al. [2] and Yu et al. [3] reviewed the method improving its performance. Shiying et al. [4] proposed a similar approach using a wavelet-based interpolating method. On the other hand, there are other methods which avoid the FBP, such as the method presented by Wang et al. [5] which considers the CT scan as a deblurring problem, and the one proposed lately by Murphy et al. [6] which tries to maximize the similarity among the data and their estimations minimizing the I-divergence.

Nevertheless, the great majority of the aforementioned software applications (to plan the dental surgery) do not have the raw data available and therefore use the backprojected data to reconstruct the patient's anatomy, so MAR methods are needed in this domain. Sohmura et al. [7] proposed a method that uses a cast of the patient's anatomy to replace the artifacted data. Tognola et al. [8] presented a method to enhance the image contrast before reconstructing the volume. In a similar way, Naranjo et al. [9] proposed a method which filters the metal artifacts in the polar domain.

The MAR methods presented above use information of the current affected slice, either its raw data or its backprojected data, to enhance itself. This paper presents a new method which uses the information of the adjoining slices of an affected one to detect its artifacted areas and remove them.

2. THE METHOD

In order to detect the artifacted areas of a slice, the method performs a comparison between the artifacted slice and a clean adjacent slice. To ensure a successful comparison two methodologies are taken into account: image registration and morphological filtering. Figure 1 shows the block diagram of the method, where I_i is the original artifacted slice and I_j is the clean image closest to I_i. The main idea of the method consists in defining a binary mask, in which the artifacted areas/pixels are set to "1" (artifacted) and the rest are set to "0" (non-artifacted). With this aim, the residue resulting from the λ-reconstruction filtering and the original artifacted image is

[*]This work has been supported by the project MIRACLE (DPI2007-66782-C03-01-AR07) of Spanish *Ministerio de Educación y Ciencia*.

[†]This work is partially supported by *Ministerio de Ciencia e Innovación*, under grant TEC2009-12675/TEC.

computed and thresholded. Only detected areas are restored by means of an inpainting method.

The residue of the λ-reconstruction filter is a morphological filter whose aim is to obtain only the artifacted areas avoiding as much as possible the anatomical structures, such as teeth or cavities, with gray level similar to the artifact. This filter needs two input images: a reference image and a marker image. The more similar the marker and the reference are, the less anatomical structures are present in the residue. For this reason, the clean slice and the artifacted one must be as close as possible. In order to increase the similarity between both images, a registration step is performed in which slice I_j is registered to I_i using a variational approach. This process obtains the marker of the morphological filter.

A brief explanation of both methodologies will be presented below. Finally, the resulting output images of the different blocks as well as the results of the algorithm, are depicted in Section 3.

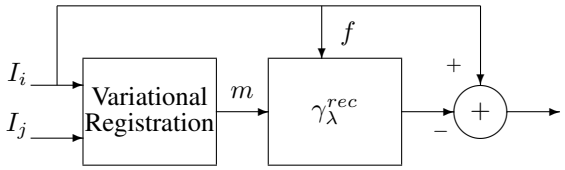

Fig. 1. Block diagram of the proposed MAR method.

2.1. Variational image registration

Image registration is the process of finding the global and/or local correspondence between two datasets (the so-named template and reference images) in such a way that the transformed template matches geometrically the reference. This task is widely used in image analysis and computer vision, having applications in various fields [10, 11]. Though its classical formulation is usually given in the spatial domain, a novel theoretical framework defined in the frequency domain is proposed in [12]. The variational minimization of the joint energy functional is performed entirely in the frequency domain, leading to a simple formulation and design, and providing more efficient implementations of the most common registration methods than the current approaches [13]. The practical implementation of this algorithm relies on a semi-implicit time-marching scheme, yielding the following iteration:

$$\mathbf{u}^{(\xi)} = \text{IFFT}\left\{\mathbf{H}\cdot\text{FFT}\{\mathbf{u}^{(\xi-1)} - \tau\cdot\mathbf{q}^{(\xi-1)}\}\right\}, \quad (1)$$

where $\mathbf{u}$ is the transformation which aligns the reference (I_i) and the template (I_j), $\mathbf{q}$ is the external forces field which drives the deformation, and $\mathbf{H} = (1+\tau\cdot\alpha\cdot\mathbf{K})^{-1}$, with $\mathbf{K} = 2\,(2-\cos(\omega_1)-\cos(\omega_2))$, $\omega_{1,2}$ being the variables in the frequency domain. In the previous expression, the notation $\mathbf{u}^{(\xi)} = \mathbf{u}(\xi\cdot\tau)$ has been used, where $\xi\in\mathbb{N}$ and $\tau>0$ are the iteration index and the time-step, respectively. Finally, the parameter $\alpha>0$, usually referred to as the regularization parameter, is a scalar which controls the smoothness of the resulting transformation.

2.2. Morphological lambda reconstruction

The λ-reconstruction operator is a family of transformations called geodesic operators [14, 15]. A geodesic operator involves two input images: the marker and the reference. A morphological transformation is applied to the marker and the gray levels of the resulting image are forced to remain above or below the reference. Let f and g (two grayscale images) be the reference and the marker images, respectively, which are both defined in the same domain as:

$$f(\mathbf{x}) : \mathrm{E} \to \mathcal{T},$$

where $(\mathbf{x})\in\mathrm{E}$ is the pixel position. In the case of valued discrete images, $\mathcal{T} = \{t_{min}, t_{min}+1, ...t_{max}\}$ (in general $\mathcal{T}\subset\mathbb{Z}$ or $\mathbb{R}$, or any compact subset of $\mathbb{Z}$ or $\mathbb{R}$) is an ordered set of grey-levels. Typically, in digital 8-bit images we have $t_{min}=0$ and $t_{max}=255$.

Let us define the unitary geodesic λ-dilation of the marker g with respect to the reference f, $\delta^{(1)}_{f,\lambda}(g)$, as the point-wise minimum between the reference and the unitary non-flat dilation, $\delta^{(1)}_{\lambda}$, of the marker, which is:

$$\delta^{(1)}_{f,\lambda}(g) = \delta^{(1)}_{\lambda}(g(\mathbf{x}))\wedge f(\mathbf{x}). \quad (2)$$

The unitary λ-dilation, $\delta^{(1)}_{\lambda}$, represents the dilation with a unitary non-flat structuring function $b(\mathbf{x})$, with $b(\mathbf{x})\in\mathcal{F}\{\mathrm{E},\mathcal{T}\}$ being a weighting function defined as:

$$b(\mathbf{x}) = \begin{cases} -\lambda & \mathbf{x}\in B \\ -\infty & \mathbf{x}\notin B \end{cases} \quad (3)$$

Thus, the unitary λ-dilation, $\delta^{(1)}_{\lambda}$, will be defined by the expression:

$$\delta^{(1)}_{\lambda}(f)(\mathbf{x}) = \{f(\mathbf{y}) : f(\mathbf{y}) = \sup[f(\mathbf{z})-\lambda], \mathbf{z}\in B_{\mathbf{x}}\}\vee f(\mathbf{x}). \quad (4)$$

The geodesic λ-dilation of size n of the marker g with respect to the reference f is obtained by performing n successive geodesic λ-dilations of g with respect to f:

$$\delta^{(n)}_{\lambda,f}(g) = \delta^{(1)}_{f,\lambda}[\delta^{(n-1)}_{f,\lambda}(g)], \quad (5)$$

with $\delta^{(0)}_{f,\lambda}(g) = g$.

The λ-reconstruction [16] of the reference image f from the marker g is defined as the geodesic λ-dilation of g with respect to f until stability:

$$\gamma^{rec}_{\lambda}(f(\mathbf{x}), g(\mathbf{x})) = \delta^{(k)}_{f,\lambda}(g(\mathbf{x})), \quad (6)$$

where k is $\delta_{f,\lambda}^{(k)}(g) = \delta_{f,\lambda}^{(k+1)}(g)$.

Using the λ-reconstruction operator, only the pixels of the reference image that match up the marker are reconstructed with the maximum value of the reference. The rest of the connected matched areas are reconstructed with an intensity level that will decrease with a slope equal to λ [17, 16].

With respect to the streaking artifact, since it has gray levels similar to the teeth and bones to which it is connected, the idea is to use the most similar image to the reference (specially in the surroundings of teeth and bones) as marker. This way, only the clear matching areas in both images will be reconstructed by the morphological filter and not the artifact, only present in the residue. The process is the same for the beam hardening, which defines a dark pattern in the surroundings of the metallic object. In this case the dual operator of the λ-reconstruction filter is used.

3. RESULTS

The method presented in this paper has been tested using several CT studies obtained using different CT scans: the GE Medical Systems HiSpeed QXi and the Philips Medical Systems CT Aura. The data have been reformatted into DICOM files. For all experiments shown in this work, the registration parameters are $\alpha = 35$, $\tau = 1$ and $\xi_{max} = 50$. With these values, the optimal performance of the registration algorithm is achieved, obtaining at the same time a likely and smooth transformation. On one hand, if a lower value of α is considered, holes or foldings could appear in the registered image. On the other hand, a high value of this regularization parameter would cause a slow convergence of the registration algorithm. The λ parameter of the morphological filter has been set to 15 in all the cases. This parameter controls the trade-off between detected and removed artifacts (true detections) and the anatomical structures wrongly detected as artifacts (false positives). The higher λ is, the more true detections and false positives are achieved.

Figure 2 shows the performance of the detection method with an illustrative example. In the first row, the figure depicts (a) an artifacted slice I_i, (b) an adjoining clean slice I_j and (c) the result of the registration of I_j and I_i, m. In the second row, the figure depicts the pairwise differences between (d) I_j and I_i using the substraction, (e) m and I_i using the substraction, and (f) m and I_i using the lambda reconstruction. As shown, the λ-reconstruction of the registered image present fewer anatomical structures.

Figure 3 shows several artifacted images (on the left), the masks obtained with the proposed method (center) and the restored image (right). For the interpolation, a linear 2D inpainting method [18] has been used.

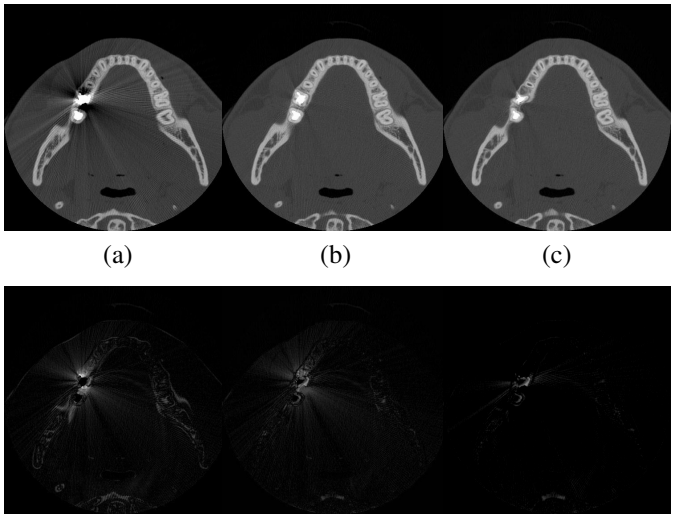

Fig. 2. (a) Original image I_i. (b) Adjacent clean slice I_j. (c) Registered image m. (d) Difference between I_i and I_j. (e) Difference between I_i and m. (f) Result of the whole method proposed in figure 1.

4. CONCLUSIONS

In this paper a new paradigm for metal artifact reduction has been proposed. The method uses a 3D approach, since it processes the information of the affected slice (horizontal plane) and also the information of adjoining slices (vertical plane). The algorithm is based on variational image registration to register the clean adjoining image to the artifacted one and the morphological λ-reconstruction to detect the artifact excluding anatomical structures such as teeth and bones. This way the artifact can be isolated and restored with non-affected data. The method has been tested on several CT studies from different CT scanners with promising results. This fact encourage us to develop new methods to reduce the false positive rates in the detection of the artifact and to test different 2D and 3D inpainting methods that provide better interpolations without giving rise to new artifacts and that can be applied on larger artifacts. Future work will also focus on automatize the method and extend it to a complete CT dataset and test it by means of 3D reconstructions of the anatomy.

5. REFERENCES

[1] W.A. Kallender, R. Hebel, and J. Ebersberger, "Reduction of CT artifacts caused by metallic implants.," *Radiology*, vol. 164, pp. 576?577, 1987.

[2] O. Watzke and W. Kallender, "A pragmatic approach to metal artifact reduction in CT: merging of metal artifact

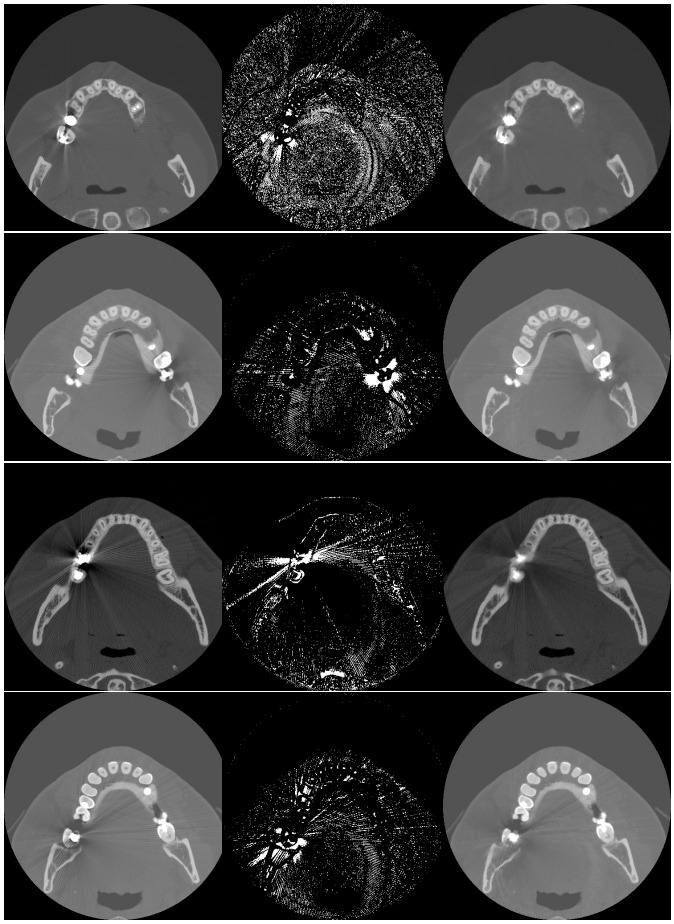

(a) (b) (c)

Fig. 3. (a) Original images. (b) Obtained masks. (c) Restored images.

reduced images," *European Radiology*, vol. 14, pp. 849–856, 2004.

[3] H. Yu, K. Zeng, G. Bharkhada, D. Wang, M. Madsen, O. Saba, B. Policeni, and W. Howard, M.and Smoker, "A segmentation-based method for metal artifact reduction," *Academic Radiology*, vol. 14, no. 4, pp. 495–504, 2007.

[4] S. Zhao, K. T. Bae, B. Whiting, and G. Wang, "A wavelet method for metal artifact reduction with multiple metallic objects in the field of view," *Journal of X-Ray Science and Technology*, vol. 10, pp. 67–76, 2002.

[5] G. Wang, D.L. Snyder, J.A. O'Sullivan, and M.W. Vannier, "Iterative deblurring for CT metal artifact reduction," *IEEE Transactions on Medical Imaging*, vol. 15, no. 5, pp. 657–664, 1996.

[6] R. Murphy, D. Snyder, D. Politte, and J. O'Sullivan, "A sieve-regularized image reconstruction algorithm with pose search in transmission tomography," in *SPIE Medical Imaging 2003: Image Processing conference*, 2003.

[7] T. Sohmura, H. Hojoh, N. Kusumoto, M. Nishida, K. Wakabayashi, and J. Takahashi, "A novel method of removing artifacts because of metallic dental restorations in 3-d ct images of jaw bone," *Clinical Oral Implant Research*, vol. 16, pp. 728 735, 2005.

[8] G. Tognola, M. Parazzini, G. Pedretti, P. Ravazzani, F. Grandori, A. Pesatori, M. Norgia, and C. Svelto, "Novel 3d reconstruction method for mandibular distraction planning," *International Workshop on Imaging Systems and Techniques*, pp. 82– 85, 2006.

[9] P. Paniagua, M. Alcaiz, V. Naranjo, R. Lloréns and S. Albalat, "A new approach in metal artifact reduction for CT 3D reconstruction," *Bioinspired Applications in Artificial and Natural Computation*, vol. 5602, 2009

[10] L. G. Brown, "A survey of image registration techniques," *ACM Computing Surveys*, vol. 24, no. 4, pp. 325–376, 1992.

[11] B. Zitová and J. Flusser, "Image registration methods: a survey," *Image and Vision Computing*, vol. 21, pp. 997–1000, 2003.

[12] J. Larrey-Ruiz, R. Verdú-Monedero, and J. Morales-Sánchez, "A Fourier domain framework for variational image registration," *J. Math. Imaging Vis.*, vol. 32, no. 1, pp. 57–72, 2008.

[13] J. Larrey-Ruiz, R. Verdú-Monedero and J. Morales-Sánchez, "Frequency implementation of the euler-lagrange equations for variational image registration.," *Signal Processing Letters*, vol. 15, pp. 321–324, 2008.

[14] J. Serra, *Image analysis and mathematical morphology*, Academic Press, 1988.

[15] P. Soille, *Morphological Image Analysis:Principles and Applications. Second Edition*, Springer, 2002.

[16] F. Meyer, "Alpha-beta flat zones, levelings and flattenings," in *Proceedings of the 6th international symposium on mathematical morphology*, 2002, pp. 47–68.

[17] V. Naranjo, A. Albiol, J.M Mossi, and Al. Albiol, "Morphological lambda-reconstruction applied to restoration of blotches in old films," in *Proceedings of the 4th IASTED International Conference on Visualisation, Imaging and Image Processing*, 2004.

[18] John D'Errico, *Inpaint-nan*, MATLAB Central File Exchange, 2005.